Fröhlich model characterization of magnetic properties of the induction heating load

Abstract

Purpose – The aim of this paper is the identification of the magnetic characteristics of the induction load by means of the B-H curve proposed by Fröhlich.

Design/methodology/approach – An electromagnetic description of the inductor system is performed to substitute the effects of the induction load, for a mathematical condition, the so-called impedance boundary condition.

Findings – A reduction of the computational cost of electromagnetic simulation through the application of the impedance boundary condition, reaching a computation time approximately 400 times faster with respect to time domain simulation. An alternative way to identify experimentally the parameters that determine the magnetic behavior of the induction load. The dependence of the equivalent impedance of an induction load on the excitation current level has been further investigated.

Practical implications – This work is performed to achieve a better understanding of the fundamentals involved in the electromagnetic modeling of an induction heating system.

Originality/value – In this paper, we introduce the dependence on the excitation level based on a first harmonic approximation and extend the impedance boundary condition to non-linear magnetic materials which allows the identification of the magnetic characteristics of the induction load.

Keywords Electromagnetism, induction heating, electromagnetic modeling, home appliances.

Paper type Research paper.

Introduction

Eddy currents are generated by placing a conductor in an electromagnetic field of medium variable frequency, and a strong variation of the fields is observed inside the material at position near to the surface (Fawzl et al., 1985). The numerical simulation of eddy current systems using numerical methods requires a very fine discretization due to the rapid decay of the fields on the surface of the conductive media. In this case, the computational cost is high and the accuracy of the results is quite limited.

With the aim of simplifying the description of the behavior of this kind of systems, the effects of the conductive medium are replaced by the so-called impedance boundary condition (IBC) (Mohsen, 1982; Yuferev, 2009), which is defined as the ratio of the tangential components of the electric and magnetic fields in the boundary between two media. This approach is particularly accurate for medium to high frequencies. The concept of IBC was introduced in (Schelkunoff, 1938) and allows to neglect the meshing of the conductor when numerical methods are applied, (Dong & Di Rienzo, 2020). Therefore, the main effect of the application of IBC is a considerable reduction of the computational cost required in the simulation of the induction heating systems. The impedance boundary condition is well-defined for linear material properties by a close expression. However, IBC expressions cannot be easily found to include some non-linearities, e.g., the magnetic saturation of the

medium (Agarwal, 1959; Del Vecchio & Ahuja, 2013; Guerin et al., 1996; Krahenbuhl et al., 1997).

This paper will commence with a concise exposition of the Fröhlich model (Bossavit & Verite, 1983; Labridis & Dokopoulos, 1989) which will be used to obtain the impedance boundary condition by numerical methods, due to the difficulty of finding a closed solution to the diffusion equation describing the behavior of the fields. Subsequently, field solutions will be computed under sinusoidal excitation, with focus placed on deriving the boundary impedance condition exclusively for the first harmonic, while higher harmonics will be disregarded. Lastly, the proposed modeling framework will be applied to a domestic induction heating (DIH) system, facilitating a comparative analysis between simulated and experimental outcomes. In DIH systems, eddy currents are primarily responsible for heating the vessels. The modeling of these pots, also referred to as induction loads, is essential as it allows for understanding the system's response under the application of external excitation. Having prior knowledge of the system's behavior allows for controlling a series of parameters such as supplied power and temperature, aiming to enhance the quality of the final product and, overall, the user experience.

Therefore, the experimentally measured results will be taken as a reference to validate the results obtained through simulation in the frequency domain. This will ultimately allow for analysing if the proposed model is appropriate and solidify the application of the impedance boundary condition as a valid method for modeling the electromagnetic properties of the induction load in DIH systems.

Induction system model
Fröhlich model
The description of a magnetic material with saturation in its B-H curve, such as the induction load, is a very complex task. Simplicity of the model is always a desirable feature, thus, a reduced number of parameters in the analytical expression of the model may be positively rated. Moreover, inaccurate results are often achieved even with the most elaborated methods. In order to address the preceding problems with a simple and reliable mathematical model, the Fröhlich saturation B-H curve has been proposed, (Labridis & Dokopoulos, 1989), whose expression is given as follows,

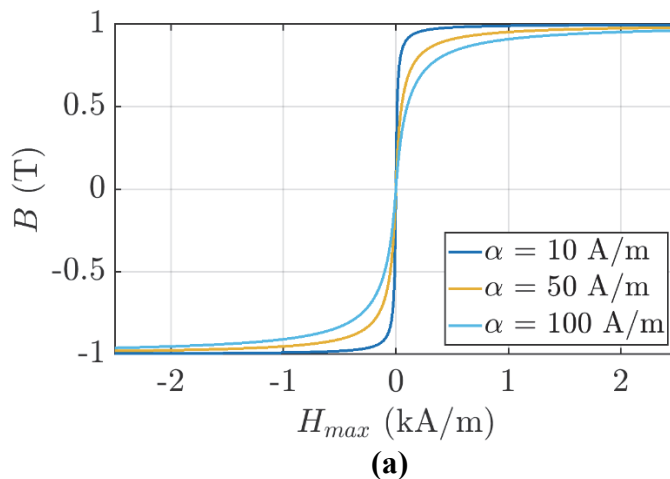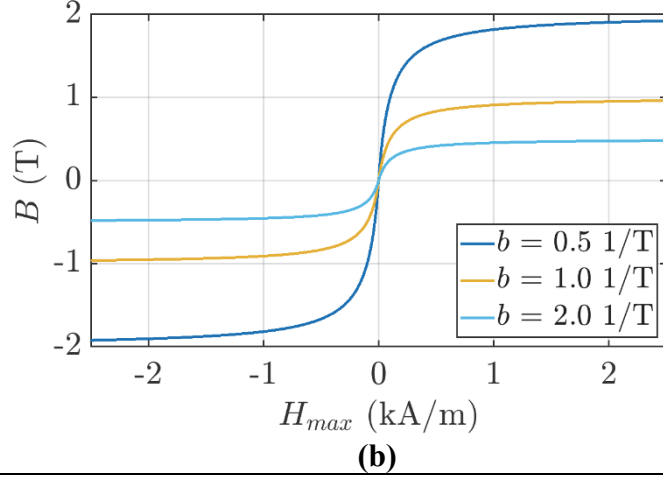$$B(H) = \frac{1}{b} \frac{H/\alpha}{1 + H/\alpha}. \tag{1}$$

(a)

Figure 1.
Dependence of the B-H curve on the Fröhlich parameters α and b.

(b)

The previous B-H relation depends exclusively on two parameters. On the one hand, the parameter b controls the saturation field level, and replacing (1) with $H \to \pm\infty$, the saturation magnetic flux field is $B_{\text{sat}} = 1/b$, as depicted in Fig. 1(b). On the other hand, the parameter α stablishes the rate at which the material becomes saturated, as it can be observed in Fig. 1(a). From expression (1), it can be noted that α introduces an effective excitation field $H_{\text{eff}} = H/\alpha$. When α is increased, more amplitude of exciting field is required to saturate the material, due to the effective field is reduced. The Fröhlich parameters α and b are characteristic of each material, both variables describe the response of the material by applying an external magnetic field.

The expression for the differential magnetic permeability, $\mu_{\text{diff}, r}(H)$, can be deduced from the derivative of the B-H curve,

$$\mu_{\text{diff}, r}(H) = \frac{1}{\mu_0} \frac{\partial B}{\partial H} = \frac{1}{\mu_0} \frac{1}{b\alpha(1 + H/\alpha)}. \tag{2}$$

where $\mu_0 = 4\pi \cdot 10^{-7}$ T·m/A is the magnetic permeability of the vacuum. The previous equation will prove useful in the following section for determining the boundary impedance condition of the induction load, as it encapsulates the non-linear magnetic characteristics of the material.

Impedance boundary condition

The impedance boundary condition (IBC) at the surface of a conductive material is given by the following relation (Fawzl et al., 1985):

$$\hat{\mathbf{n}} \times \mathbf{E} = Z_{\text{IBC}} \cdot \hat{\mathbf{n}} \times (\hat{\mathbf{n}} \times \mathbf{H}), \tag{3}$$

where $\hat{\mathbf{n}}$ is the unitary normal vector out of the conductor. The preceding expression enforces a relationship between the tangential electric and magnetic fields at the conductor surface. Assuming that fields exhibit a time dependence $e^{j\omega t}$ which corresponds to an oscillation of angular frequency ω, the tangential components of the electric and magnetic fields in the surface are perpendicular. Selecting the adequate reference system, the normal vector can be expressed along z-direction,

whereas the electric field amplitude E_x and magnetic field amplitude H_y are along the x-direction and y-direction, respectively. In the latter case, the impedance boundary condition, Z_{IBC}, is defined as:

$$Z_{IBC} = \frac{E_x}{H_y}\bigg|_{z=0}. \tag{4}$$

The relationship (4) for the IBC in linear media can be deduced analytically by using the Maxwell-Ampère equation with a magneto-quasi-static approach (Carretero et al., 2011; Özakın & Aksoy, 2016). This approximation leads to neglecting the displacement currents i.e., $\mathbf{J}_D = \partial \mathbf{D}/\partial t \approx \mathbf{0}$, which is an accurate assumption at the working frequencies of induction heating systems. Thus, the linear impedance boundary condition, Z_{IBC}, can be expressed as:

$$Z_{IBC} = \frac{1+j}{\sigma \delta} = \frac{\sqrt{2}}{\sigma \delta} e^{j\frac{\pi}{4}}. \tag{5}$$

where σ and μ are the electrical conductivity and magnetic permeability of the material. The skin depth $\delta = \sqrt{2/\omega\mu\sigma}$ (Bay et al., 2003; Wentworth et al., 2006; Wheeler, 1942) represents the characteristic distance of the exponential decaying of the fields inside the medium. In this scenario, accurate results are obtained by substituting the conductor domain with this boundary condition when the skin depth is significantly smaller than the dimensions of the system, this is directly related to the magneto-quasi-static approximation applied previously, as the penetration depth depends on the frequency. The preceding relationship establishes that the electric and magnetic fields are 45° out of phase at the surface of a conductor material, being these characteristics independent on the physical properties of the medium or the operating frequency. In addition, the ratio between the amplitudes of the fields at the surface depends on the physical properties as well as the frequency but it is independent on the exciting field amplitude.

However, under nonlinear magnetic material properties, such as those encountered with magnetic saturation, which is the case for the induction loads, a closed expression of the IBC cannot be derived. The fields distribution within a nonlinear magnetic material will be obtained by applying the following diffusion equation, (Jufer & Apostolides, 1976):

$$\frac{1}{\sigma}\nabla^2 H = \frac{\partial B}{\partial H}\frac{\partial H}{\partial t}. \tag{6}$$

The previous expression can be simplified by considering that the diffusion direction, z, is the direction of maximum variation of the fields penetrating the conductor. Therefore, the plane-wave assumption is adopted to approximate the Laplacian operator as $\nabla^2 H \approx \partial^2 H/\partial z^2$ and the nonlinear B-H curve is incorporated by the factor $\mu_{diff}(H) = \partial B/\partial H$ which is given by the analytical differential permeability provided in (2) within the Fröhlich model. Thus, expression (6) becomes:

$$\frac{\partial H}{\partial t} = \frac{1}{\sigma \mu_{\text{diff}}(H)} \frac{\partial^2 H}{\partial z^2}. \tag{7}$$

The preceding non-linear diffusion equation is analytically unsolvable. Numerical methods are therefore applied to obtain valid solutions. In this work, a finite difference method (FDM) (Jufer & Apostolides, 1976) was applied due to its good trade-off between complexity and accuracy. In order to ensure convergence, an unstructured mesh implicit method (Carretero et al., 2024) was employed and whose solution corresponds to the spatial-temporal magnetic field, $H_y(z,t)$, inside the conductor material. The constraints $H_y(z=0,t) = H_0 \sin(\omega t)$ and $H_y(z=z_{\text{max}},t) = 0$ are applied varying the amplitude H_0. In addition, the electric field $E_x(z,t)$ can be deduced by applying Ohm's and Ampère laws:

$$E_x(z,t) = -\frac{1}{\sigma}\left(\frac{\partial H_y(z,t)}{\partial z}\right). \tag{8}$$

Furthermore, when subjected to harmonic magnetic field excitation, the electric field $E_x(z,t)$ comprises not only the first harmonic but also higher harmonics. Depending on the degree of nonlinearity, the significance of these higher harmonics can vary. While the non-linear impedance boundary condition cannot be precisely defined, the first harmonic approach will be considered as follows:

$$Z_{\text{IBC}}^{\text{NL}} = \left.\frac{E_x^1}{H_y^1}\right|_{z=0}, \tag{9}$$

where E_x^1 and H_y^1 are the first harmonic of the transversal components of the electric and magnetic fields at the conductor surface, respectively, extracted by means of the discrete Fourier transform (Apolinário & Diniz, 2014; Sevgi, 2014). On the contrary to linear media, the non-linear IBC depends on the excitation field level, $Z_{\text{IBC}}^{\text{NL}} = Z_{\text{IBC}}^{\text{NL}}(H)$.
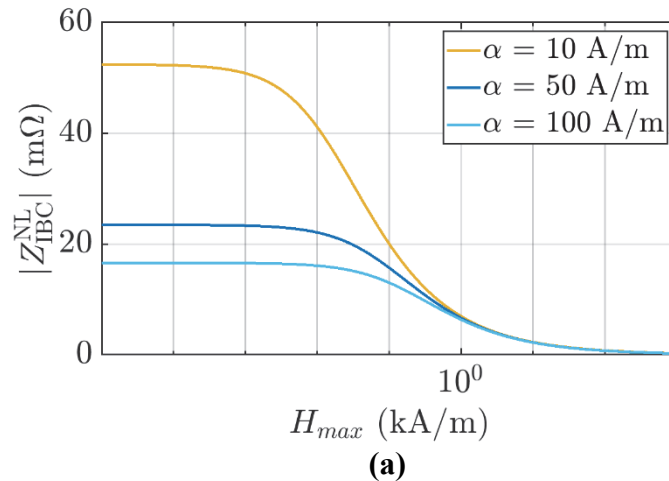

Figure 2. Impedance boundary condition Z_{IBC} at different Fröhlich parameters α: (a) modulus $|Z_{\text{IBC}}|$, (b) phase $\angle Z_{\text{IBC}}$.
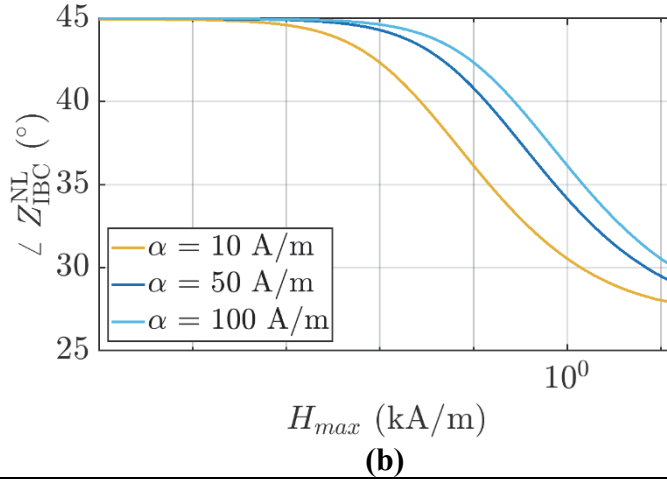
(b)

Fig. 2 and Fig. 3 depict the non-linear impedance boundary condition $Z_{\text{IBC}}^{\text{NL}}(\alpha,b)$ in relation to the field amplitude for a Fröhlich B-H curve. As it can be seen, at small signal levels, non-linear IBC is equal to the linear IBC considering the initial permeability of the material, but, increasing the excitation field level, the modulus and the phase of the non-linear IBC decrease, on the contrary to the linear material behavior. Moreover, the absolute value of the non-linear IBC depends on the parameter b but the phase is independent on it. Conversely, the parameter α influences both modulus and phase of the non-linear IBC.
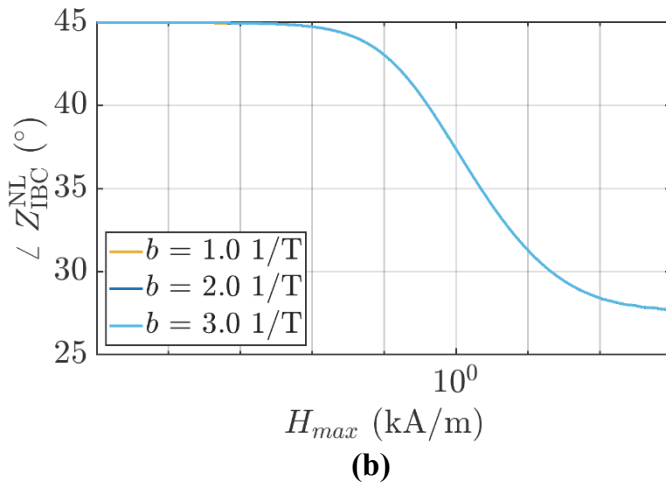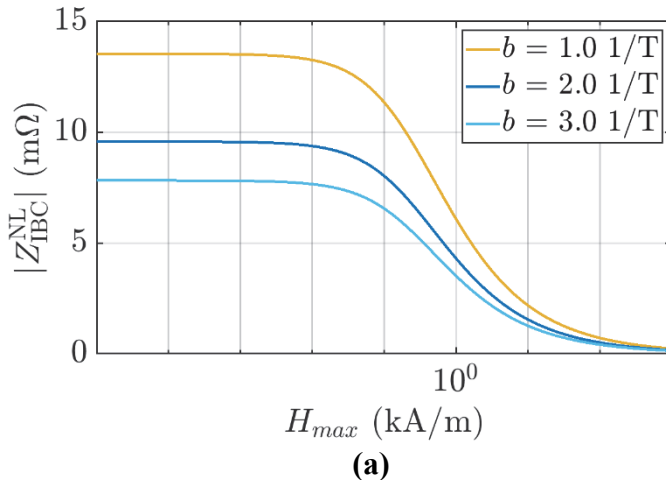

(a)

(b)

Figure 3. Impedance boundary condition Z_{IBC} at different Fröhlich parameters b : (a) modulus $\left|Z_{\text{IBC}}\right|$, (b) phase $\angle Z_{\text{IBC}}$.

Simulation Model

The expression of the IBC based on a Fröhlich B-H curve will be employed to model the induction load. The advantage of using this approach is twofold: firstly, the load meshing is avoided, which thereby reducing computational cost; secondly, the dependence behavior with the excitation level is captured. Although the geometry of the reference system is simple, a commercial FEA simulation tool will be used, i.e., COMSOL® (COMSOL Multiphysics Programming Reference Manual, 1998), in order to consider the proposed modelling for other complex induction heating system.

Figure 4.
2D-axisymmetric model of the induction heating system.
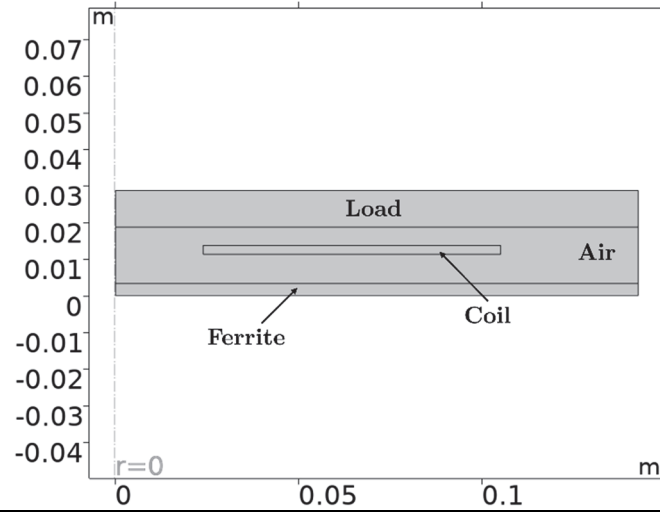
The reference system shown in Fig. 4 consists of a spiral inductor composed of $n = 23$ turns evenly distributed between the internal radius $r_{int} = 20$ mm and the external radius $r_{ext} = 105$ mm. The thickness of the coil is $t_{coil} = 2.3$ mm. The coil is placed a distance $d_f = 3$ mm above the flux concentrator plate composed of high-permeability ferrite. The load is located at a distance of $d_l = 4.5$ mm above the coil.

The physical configuration of the FEA tool model is performed by bearing in mind simplicity. The coil is modelled by an impressed constant current density assuming the homogenization of the turns into the cross-section area of the coil, $\mathbf{J}_{coil} = nI_0 / S_{coil}\hat{\boldsymbol{\varphi}}$, directed along the azimuthal axis, where I_0 is the current amplitude and $S_{coil} = t_{coil}(r_{ext} - r_{int})$. The flux concentrator is substituted by the Perfect Magnetic Conductor or $\hat{\mathbf{n}} \times \mathbf{H} = \mathbf{0}$ (Lindell & Sihvola, 2020; Orton & Seddon, 2003) in its surface, being the preceding condition equivalent to an infinite relative permeability of the ferrite. Finally, the non-linear impedance boundary condition is applied to the surface of the induction load.

A coarse meshing is implemented to the model because the fields exhibit a smooth spatial dependence on the domains simulated. Also, the numerical results have been calculated in the frequency-domain. The model presents a high accuracy at a low computational cost; thus, multiple configurations can be simulated with reduced computational cost. The equivalent impedance of the induction load, denoted as Z_{ind}, can be readily determined from the simulated results, particularly from the induced coil voltage, V_{coil}, which is computed by integrating the azimuthal

component of the electric field along the coil turns, (Carretero et al., 2012). In the frequency domain, the induced voltage is complex-valued, thus, the equivalent impedance $Z_{ind} = V_{coil} / I_0$ is also complex-valued. The real part of the equivalent impedance corresponds to the equivalent resistance of the induction system and the imaginary component is associated with its equivalent inductance. Not only does impedance vary with frequency, but it also exhibits a dependency on current amplitude, stemming from alterations in the load's magnetic properties in response to the excitation field strength. Therefore, the equivalent impedance with the dependencies described above can be decomposed into resistive and inductive contributions $Z_{ind}\left(\omega, \hat{I}\right) = R + j\omega L$. The resistance models the dissipation of transferred power and the inductance takes into account the magnetic energy stored in the system.

Experimental results

In order to prove the feasibility of the proposed modelling of inductive heating systems based on impedance boundary condition from Fröhlich B-H curve, some experimental measurements have been conducted. The experimental set-up consists of a spiral coil of $n = 23$ turns placed over a rectangular ferrite plane. The load of the induction heating system is a pot of enamelled magnetic iron. The induction heating system is fed-up by a resonant converter connected to the mains. The electronics are composed of an ac-dc converter which rectifies the voltage of the mains, then, a modulated dc-bus is generated, v_{bus}. Next, a half-bridge inverter provides a pulsed voltage between 0 V and v_{bus}, working at the switching frequency f_{sw} to the resonant tank composed of the induction-load system and the matching network. The current through the coil is modulated by the dc-voltage v_{bus} and the first-harmonic of the switching frequency f_{sw} is the dominant.

The experimental set-up consists of a power converter connected to an inductor-load system. The power converter is controlled by an open-loop software. Current and voltage in the coil have been measured by means of a Tektronix DPO7354 oscilloscope, using a Pearson current probe and a differential voltage probe, respectively. Data have been stored to be processed in MATLAB®. Harmonics of waveforms have been extracted by applying the Fourier analysis at each switching period, as well as other parameters of interest, e.g., the current amplitude for each period. Equivalent impedance for each switching period were calculated by the ratio between the complex-valued first-harmonic inductor voltage and the current.

The magnetic properties of the induction load, i.e., magnetic iron, have been identified from the experimental measurements by fitting Fröhlich parameters α and b to several equivalent impedance at key current levels. The measured equivalent impedances at 35 kHz have been chosen for the identification of the parameters. Equivalent impedances at small currents have been discarded because the behavior of the load cannot be explained by the proposed model. An iterative algorithm based on FDM extraction of the $Z_{IBC}\left(H, \alpha, b\right)$, $Z_{ind}\left(\omega, \hat{I}\right) = R + j\omega L$ calculation in COMSOL® and adaptive gradient (Kingma & Ba, 2014; Kochenderfer & Wheeler, 2019; Zaheer & Shaziya, 2019) descend has been used to obtain the values of α and b. Thus, assuming a typical iron electrical conductivity $\sigma = 1.12 \cdot 10^7$ S/m and a fixed temperature of 100ºC (boiling point of water), the Fröhlich parameters obtained for the enamelled ferromagnetic load are $\alpha = 151.21$ A/m and $b = 0.34$ 1/T.

A comparison between the measured equivalent resistance with respect to the current amplitude and the values calculated from the FEA tool for the preceding Fröhlich values are given in Fig. 5(a). Besides, a similar comparison is given for the equivalent inductance in Fig. 5(b). Two different switching frequencies of 30 and 45 kHz, respectively are represented for each electrical parameter. As it can be seen, a good accuracy is achieved by the modelling because the maximum resistance error is around 6%, whereas the maximum inductance error is around 3% at 30 kHz. At the frequency of 45 kHz, lower current amplitudes are reached because the resonance frequency can be found below 30 kHz. Due to the appearance of higher order harmonics with increasing frequency, the error in both resistance and inductance is higher. Related to this, the main source of error between experimental measurements and simulation data is the first harmonic approximation in the IBC calculation.
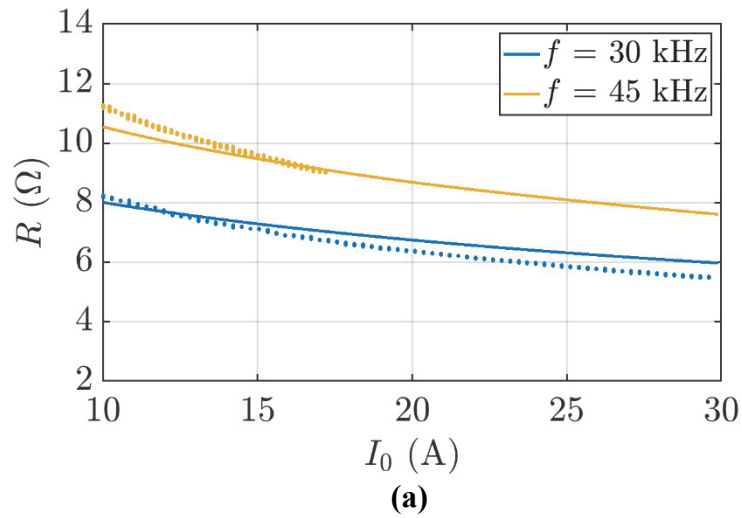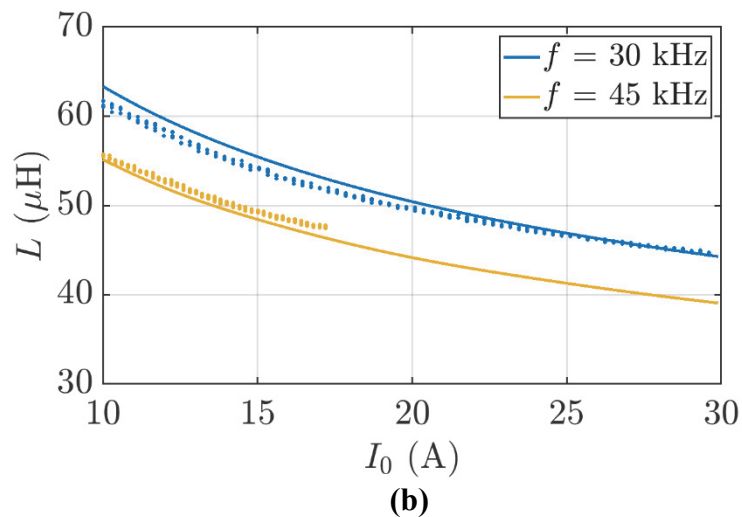

Figure 5.
Comparison between experimental equivalent impedance and the simulated values from the Fröhlich model with respect to the current amplitude at 30 kHz and 45 kHz (lines: simulation results; points: experimental data): (a) equivalent resistance, (b) equivalent inductance.

From the proposed modeling based on the impedance boundary condition of the Fröhlich B-H curve, the dependence on the current of the equivalent impedance can be explained associated with the magnetic saturation of the material. Therefore, the aforementioned non-linear IBC extend the accuracy of the frequency domain simulation of induction heating systems.

It is worth noting that, despite using a simple model for the electromagnetic simulation of the DIH system, reasonable results have been achieved, and the behavior of the induction load has been satisfactorily captured. This suggests that

increasing the complexity of the model may not necessarily yield results that justify the considerable increase in computational cost required by such simulations.

Conclusions

In this work, the potential of the IBC extracted from the Fröhlich model has been explored. As the most important result, the dependence of the equivalent impedance of an induction load on the excitation current level has been further investigated. Typical linear IBC is derived from only a single magnetic property parameter, namely, relative permeability of the material, but, the proposed model just extends the magnetic properties to two parameters including saturation effects. Consequently, the B-H curve remains simple but increasing the explanatory power of the modelling.

The application of the proposed Fröhlich B-H curve-based impedance boundary condition implies a slightly increase in the computational cost of the simulation with respect to the linear IBC feature included in commercial FEA tools. However, the proposed method also allows frequency domain simulation, therefore, complex system geometries can be simulated.

The experimental validation has proven the feasibility of the proposed non-linear modeling, because the error in the estimated components of the equivalent impedances is small under different configurations.

References

Agarwal, P. D. (1959). Eddy-current losses in solid and laminated iron. *Transactions of the American Institute of Electrical Engineers, Part I: Communication and Electronics*, *78*(2), 169–181. https://doi.org/10.1109/TCE.1959.6372977

Apolinário, I., & Diniz, P. (2014). Chapter 1. Introduction to Signal Processing Theory. *Academic Press Library in Signal Processing*, *1*. https://doi.org/10.1016/B978-0-12-396502-8.00001-2

Bay, F., Labbe, V., Favennec, Y., & Chenot, J. L. (2003). A numerical model for induction heating processes coupling electromagnetism and thermomechanics. *International Journal for Numerical Methods in Engineering*, *58*(6), 839–867. https://doi.org/10.1002/nme.796

Bossavit, A., & Verite, J. (1983). The "TRIFOU" Code: Solving the 3-D eddy-currents problem by using H as state variable. *IEEE Transactions on Magnetics*, *19*(6), 2465–2470. https://doi.org/10.1109/TMAG.1983.1062817

Carretero, C., Acero, J., & Burdio, J. M. (2024). Normalized nonlinear impedance boundary condition in anhysteretic magnetic material for eddy current problems. *IEEE Transactions on Magnetics, doi: 10.1109/TMAG.2024.3395924.*

Carretero, C., Luca, Ó., Acero, J., Alonso, R., & Burdío, J. M. (2011). An application of the impedance boundary condition for the design of coils used in domestic induction heating systems. *COMPEL - The International Journal for Computation and Mathematics in Electrical and Electronic Engineering*, *30*(5), 1616–1625. https://doi.org/10.1108/03321641111152775

Carretero, C., Lucia, O., Acero, J., Alonso, R., & Burdio, J. M. (2012). Frequency-dependent modelling of domestic induction heating systems using numerical methods for accurate time-domain simulation. *IET Power Electronics*, *5*(8), 1291–1297. https://doi.org/10.1049/iet-pel.2012.0113

COMSOL Multiphysics Programming Reference Manual. (1998). www.comsol.com/blogs

Del Vecchio, R. M., & Ahuja, R. (2013). Analytic nonlinear correction to the impedance boundary condition. *IEEE Transactions on Magnetics*, *49*(12), 5687–5691. https://doi.org/10.1109/TMAG.2013.2273891

Dong, J., & Di Rienzo, L. (2020). FEM and BEM implementations of a high order surface impedance boundary condition for three-dimensional eddy current problems. *IEEE Access*, *8*, 186496–186504. https://doi.org/10.1109/ACCESS.2020.3029566

Fawzl, T. H., Ahmed, M. T., & Burke, P. E. (1985). On the use of the impedance boundary conditions in eddy current problems. *IEEE Transactions on Magnetics*, *21*(5), 1835–1840. https://doi.org/10.1109/TMAG.1985.1063920

Guerin, C., Meunier, G., & Tanneau, G. (1996). Surface impedance for 3D nonlinear eddy current problems-application to loss computation in transformers. *IEEE Transactions on Magnetics*, *32*(3), 808–811. https://doi.org/10.1109/20.497364

Jufer, M., & Apostolides, A. (1976). An analysis of eddy current and hysteresis losses in solid iron based upon simulation of saturation and hysteresis characteristics. *IEEE Transactions on Power Apparatus and Systems*, *95*(6), 1786–1794. https://doi.org/10.1109/T-PAS.1976.32279

Kingma, D. P., & Ba, J. (2014). *Adam: A Method for Stochastic Optimization*. http://arxiv.org/abs/1412.6980

Kochenderfer, M. J., & Wheeler, T. A. (2019). *Algorithms for Optimization*. http://mitpress.mit.edu.

Krahenbuhl, L., Fabregue, O., Wanser, S., De Sousa Dias, M., & Nicolas, A. (1997). Surface impedances, BIEM and FEM coupled with 1D non-linear solutions to solve 3D high frequency eddy current problems. *IEEE Transactions on Magnetics*, *33*(2), 1167–1172. https://doi.org/10.1109/20.582461

Labridis, D., & Dokopoulos, P. (1989). Calculation of Eddy Current Losses in Nonlinear Ferromagnetic Materials. *IEEE Transactions on Magnetics*, *25*(3), 2665–2669. https://doi.org/10.1109/20.24506

Lindell, I. V, & Sihvola, A. (2020). Perfect Electromagnetic Conductor Boundary. In *Boundary Conditions in Electromagnetics* (pp. 11–31). https://doi.org/10.1002/9781119632429.ch2

Mohsen, A. (1982). On the impedance boundary condition. *Applied Mathematical Modelling*, *6*(5), 405–407.

Orton, R. S., & Seddon, N. J. (2003). PMC as an antenna structural component. *Twelfth International Conference on Antennas and Propagation, 2003 (ICAP 2003). (Conf. Publ. No. 491)*, *2*, 599–602 vol.2. https://doi.org/10.1049/cp:20030146

Özakın, M. B., & Aksoy, S. (2016). Application of Magneto-Quasi-Static Approximation in the Finite Difference Time Domain Method. *IEEE Transactions on Magnetics*, *52*(8), 1–9. https://doi.org/10.1109/TMAG.2016.2535415

Schelkunoff, S. A. (1938). The Impedance Concept and Its Application to Problems of Reflection, Refraction, Shielding and Power Absorption. *Bell System Technical Journal*, *17*(1), 17–48. https://doi.org/https://doi.org/10.1002/j.1538-7305.1938.tb00774.x

Sevgi, L. (2014). Fourier Transform and Fourier Series. In *Electromagnetic Modeling and Simulation* (pp. 71–94). https://doi.org/10.1002/9781118716410.ch4

Wentworth, S. M., Baginski, M. E., Faircloth, D. L., Rao, S. M., & Riggs, L. S. (2006). Calculating Effective Skin Depth for Thin Conductive Sheets. *2006*

IEEE Antennas and Propagation Society International Symposium, 4845–4848. https://doi.org/10.1109/APS.2006.1711728

Wheeler, H. A. (1942). Formulas for the Skin Effect. *Proceedings of the IRE, 30*(9), 412–424. https://doi.org/10.1109/JRPROC.1942.232015

Yuferev, S. V. (2009). Surface Impedance Boundary Conditions. In *Surface Impedance Boundary Conditions*. https://doi.org/10.1201/9781315219929

Zaheer, R., & Shaziya, H. (2019). A Study of the Optimization Algorithms in Deep Learning. *Proceedings of the 3rd International Conference on Inventive Systems and Control, ICISC 2019,* 536–539. https://doi.org/10.1109/ICISC44355.2019.9036442